



The effect of expansion ratio for creeping expansion flows of UCM fluids

R.J. Poole^a, F.T. Pinho^{b,*}, M.A. Alves^c, P.J. Oliveira^d

^a Department of Engineering, University of Liverpool, Brownlow Street, Liverpool L69 3GH, United Kingdom

^b Departamento de Engenharia Mecânica, CEFT, Faculdade de Engenharia da Universidade do Porto, Rua Dr. Roberto Frias, 4200-465 Porto, Portugal

^c Departamento de Engenharia Química, CEFT, Faculdade de Engenharia da Universidade do Porto, Rua Dr. Roberto Frias, 4200-465 Porto, Portugal

^d Departamento de Engenharia Electromecânica, Unidade Materiais Têxteis e Papeleiros, Universidade da Beira Interior, 6201-001 Covilhã, Portugal

ARTICLE INFO

Article history:

Received 4 February 2009

Received in revised form 19 May 2009

Accepted 15 June 2009

Keywords:

Planar sudden expansion

UCM

Creeping flow

Expansion ratio effects

ABSTRACT

A systematic numerical investigation on creeping flows in planar sudden expansions of viscoelastic fluids obeying the upper-convected Maxwell model is carried out to assess the combined effects of viscoelasticity, through the Deborah number, and expansion ratio (ER), which was varied between 1.25 and 32. At large expansion ratios ($ER \geq 4$) the flow becomes dominated by the downstream duct size and appropriately normalized quantities tend to be independent of ER. The recirculation size and strength become decreasing functions of De , whereas the Couette correction (the normalized entry pressure drop due to the presence of the expansion) increases. At small ER ($ER \leq 3$), however, no simple scaling laws are found and there is a complex interaction between De and ER leading to non-monotonic variations, with an initial decrease in the recirculation length at low Deborah numbers, followed by an enhancement as De increases.

© 2009 Elsevier B.V. All rights reserved.

1. Introduction

Sudden expansion flows have been the topic of many investigations for Newtonian fluids, in particular under turbulent-flow conditions, where the flow is simultaneously geometrically simple and dynamically complex with shear and extensional flow regions in combination with all the mechanisms of turbulent production, dissipation and diffusion [1]. Most of these Newtonian turbulent works are concerned with the corresponding axisymmetric geometry [2,3] given their easier construction and inherent symmetry. Limited results for viscoelastic fluids in turbulent flow have also been reported in both planar [4] and axisymmetric geometries [5–7].

Investigations under laminar flow conditions have also been conducted especially aimed at exploring the asymmetric flow characteristics in two-dimensional or three-dimensional channels [8–10]. This has obviously motivated the corresponding research with non-Newtonian fluids [11–14], but there are also works aimed at simply determining pressure-loss coefficients for engineering purposes [15]. However, these non-Newtonian investigations, as well as others reviewed by Poole et al. [16], are under conditions of non-negligible inertia.

In this work we want to tackle planar expansion flows under conditions of vanishing inertia typical of polymer processing opera-

tions. In their two-dimensional numerical investigation on creeping flows in a 1:3 plane sudden expansion (expansion ratio, $ER = D/d = 3$, where D and d are the large and small half-channel widths) for upper-convected Maxwell (UCM) and Oldroyd-B (Old-B) fluids, using refined meshes and higher-order discretization schemes, Poole et al. [16] found that fluid elasticity reduced the length of the recirculation (X_R) by less than 20% relative to the corresponding Newtonian flow. Simultaneously, the strength of these recirculations as measured by the recirculating flow rate was reduced by 60%. These findings were in contrast to the results of previous research, which predicted the elimination of the recirculation region as viscoelastic normal stresses increased with Deborah number [17,18]. The results of Poole et al. [16] for the Phan-Thien–Tanner (PTT) model were even more dramatic, because after an initial decrease in X_R at low Deborah numbers, X_R increased for $De > 15$, while the recirculation intensity stabilized to about 35% of the corresponding Newtonian value. Whereas these simulations relied on refined meshes and high-resolution differencing schemes, the early predictions of [17] were carried out on very coarse meshes, while [18] used coarse meshes together with a first-order interpolation scheme for advection.

Those simulations of Poole et al. [16] were for a single, fixed expansion ratio $ER = 3$ and also reported the onset of a “lip vortex” in the upstream channel, near the singularity (re-entrant corner), for the UCM and Old-B fluids and the corresponding “converging streamlines” phenomenon. The authors attributed these converging streamlines to the increase in X_R , outweighing at higher Deborah number the competing effect of the normal stresses, which precluded the continuous decrease in the recirculation length with

* Corresponding author. Tel: +351 22 508 1597; fax: +351 22 508 1440.

E-mail addresses: robpoole@liv.ac.uk (R.J. Poole), fpinho@fe.up.pt (F.T. Pinho), mmalves@fe.up.pt (M.A. Alves), pjpo@ubi.pt (P.J. Oliveira).

De. Clearly, the sudden expansion flow is more complex than initially thought on account of its geometric singularity, which is also responsible for convergence difficulties in more complex flows containing sudden expansions as found by Afonso and Pinho [19].

The present investigation is a follow-up to the work of Poole et al. [16] to further explore and understand the flow dynamics of UCM fluids in plane sudden expansions and in particular with an assessment of the effects of expansion ratio, which is here varied between 1.25 and 32. Although such high expansion ratios are rare in actual processing operations involving polymers there is the need, from a fundamental point of view, to understand the vortex evolution for a wide range of geometrical and flow conditions. In this work we find that the behavior reported previously regarding the attenuation of vortex activity by viscoelasticity is in fact not unique [16] being only typical of moderate to large ($ER > 2$) expansion ratios. For expansion ratios below 3 the variation of X_R with *De* is non-monotonic, showing first a decrease followed by an increase in X_R , with the minimum X_R condition taking place at Deborah numbers well below 1. This more extensive characterization of viscoelastic flows and the information and data provided by the present study, in particular the vortex size and intensity as a function of *De* number (that is, flow rate) and the pressure drop due to the expansion may be useful for the practical design of processing equipment in addition to their use for benchmarking purposes. In addition the contraction–expansion geometry is a well-known benchmark and studying the expansion in isolation may help in the understanding of this problem for example in illuminating the contribution of the expansion in the overall enhanced pressure drop.

In the remaining of this paper we briefly present the governing equations and the numerical method (Section 2), then in Section 3 the geometries and computational meshes are described and the results are presented and discussed in Section 4, prior to closure.

2. Governing equations and numerical method

The flow under investigation is laminar and the fluid is assumed incompressible leading to the following mass conservation equation and momentum transport equation (creeping flow), respectively:

$$\nabla \cdot \mathbf{u} = 0, \quad (1)$$

$$-\nabla p + \nabla \cdot \boldsymbol{\tau} = 0. \quad (2)$$

Here, \mathbf{u} is the velocity vector, p is the pressure and $\boldsymbol{\tau}$ is the extra stress tensor described by Eq. (3), the rheological constitutive equation for the UCM model [20], where λ and η are the relaxation time and viscosity coefficient, respectively

$$\lambda \left[\frac{\partial \boldsymbol{\tau}}{\partial t} + \nabla \cdot \mathbf{u} \boldsymbol{\tau} - \boldsymbol{\tau} \cdot \nabla \mathbf{u} - \nabla \mathbf{u}^T \cdot \boldsymbol{\tau} \right] + \boldsymbol{\tau} = \eta (\nabla \mathbf{u} + \nabla \mathbf{u}^T). \quad (3)$$

These equations, and the corresponding results of simulations, can be made non-dimensional through the introduction of appropriate reference length (L) and velocity (U) scales, and the Deborah number ($De = \lambda U/L$) in Eq. (3), which are defined in the next section.

The finite-volume numerical method used to solve Eqs. (1)–(3) is the same used by Poole et al. [16] and has been described in detail elsewhere [21], so only a very brief outline is given here. The numerical method is based on a time-marching version of the SIM- PLEC pressure correction algorithm formulated with the collocated variable arrangement. The governing equations are integrated in space over each of the computational cells of the mesh, and in time over a time step, to form sets of linearised algebraic equations. The discretization of the governing equations is based on central differences for diffusion terms and for convective terms the interpolating scheme employed is CUBISTA [22], a high-resolution scheme especially devised for convective terms in constitutive equations,

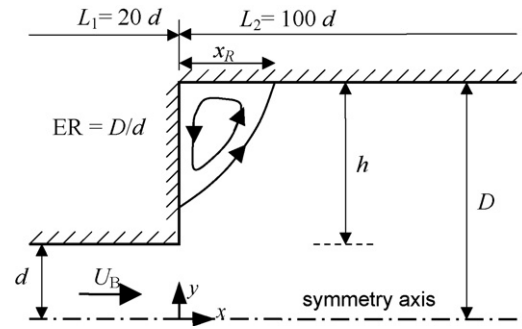


Fig. 1. Schematic representation of the expansion geometry.

which is formally of third order accuracy in uniform meshes. The steady solutions were obtained by time-marching the equations using the implicit Euler method, an unconditionally stable first-order scheme. This method does not affect the accuracy of the results of the steady solutions.

3. Geometry, computational meshes and numerical accuracy

A schematic of the expansion geometry is shown in Fig. 1. The inlet channel of half-width d is kept constant regardless of the expansion ratio. The half-width of the expansion channel is D and the expansion ratio is defined as $ER = D/d$. At the inlet fully developed velocity and stress profiles were imposed as boundary conditions and the inlet channel length was 20 times the inlet half-width. Neumann boundary conditions were imposed to velocities, stresses and the pressure gradient at the outflow and the outlet channel length was long ($L_2 = 100d$) to eliminate any possible interference of the outlet in the expansion region flow kinematics. Imposition of zero streamwise gradients of the extra stress is consistent with the first-order derivative constitutive equations here employed for which there is no need to give any outlet boundary condition. The transportive property of the CUBISTA scheme and the Neumann conditions effectively disconnect the inner grid points from the stresses existing at the outlet plane, thus preserving the physics inherent to the constitutive equations.

Only half of the domain was mapped given the symmetry of the flow. This is a reasonable modeling assumption, because flow asymmetries for viscoelastic fluids in these geometries have been observed by Oliveira [12] to take place only at Reynolds numbers larger than 1, whereas here we are simulating creeping flows. Indeed, calculations mapping the whole domain, not reported here, confirmed the essential symmetry of the flow.

For consistency with the literature, the non-dimensional Deborah (*De*) number is defined on the basis of the upstream channel characteristics and given by $De = \lambda U_B/d$, where U_B is the mean inlet velocity, also called bulk velocity, in the upstream channel. This is consistent with taking the upstream mean velocity and half-width as characteristic velocity ($U \equiv U_B$) and length ($L \equiv d$) scales, respectively.

For some geometries computations were carried out in two meshes the finer of which has a degree of fineness of the order of mesh M3 in Poole et al. [16], but with a number of cells intermediate to their meshes M2 and M3. The meshes used are non-uniform to allow local refinement, as in [16], with increased concentration of cells around the protruding corner of the expansion geometry, and their characteristics are listed in Table 1, giving the total number of cells, the number of degrees of freedom (DOF), the maximum rate of cell size variation ($f_x = \Delta x_i / \Delta x_{i-1}$) and the smallest cell spacing. Results of calculations allowed the assessment of numerical accuracy as listed in Table 2. The numerical uncer-

Table 1
Characteristics of the computational meshes.

	NC	DOF	$(\Delta x)_{\min}/d$	$f_{x,\max}$
ER = 1.25				
M1	17,500	105,000	0.0025	1.0846
M2	70,000	420,000	0.00125	1.0414
ER = 1.5				
M1	14,500	87,000	0.0025	1.076
M2	58,000	348,000	0.00125	1.0373
ER = 2				
M1	14,500	87,000	0.005	1.076
M2	58,000	348,000	0.0025	1.0373
ER = 4				
M1	15,000	90,000	0.01	1.072
M2	60,000	360,000	0.005	1.0354
ER = 8				
M1	21,500	129,000	0.01	1.0673
M2	86,000	516,000	0.005	1.0331
ER = 16				
M1	21,500	129,000	0.01	1.0673
M2	86,000	516,000	0.005	1.0331
ER = 32				
M1	21,500	129,000	0.01	1.070
M2	86,000	516,000	0.005	1.0344

tainties of the computations with mesh M2, used to perform all subsequent computations in this work, are listed in Table 2 except for ER=3 where data from [16] was used. The uncertainty in x_R is less than 0.1% for Newtonian fluids, but for the UCM fluid it increases with Deborah number and the worst case is obtained at the highest Deborah number of 1 at ER=1.5, but not exceeding 0.6%. The uncertainty is determined in relation to the extrapolated value (x_R^*) calculated with Richardson's extrapolation technique ($x_R^* = (2^p x_{R2} - x_{R1}) / (2^p - 1)$ where x_{R1} and x_{R2} are the values of x_R on meshes M1 and M2, respectively) assuming that the order of convergence is $p = 2$ (this order is based on similar computations of Poole et al. [16] for ER=3 using three meshes). Thus, the uncertainty in x_R is $e(x_R) = |x_{R2} - x_R^*| / x_R^* \times 100\%$. As an example of calculation, at $De = 1$ and ER=4 the recirculation size $X_R = x_R/d$ obtained on meshes M1 and M2 were: $X_{R1} = 1.2339$ and $X_{R2} = 1.2303$; Richardson extrapolation gives $X_R^* = (4X_{R2} - X_{R1})/3 = 1.2291$ and the uncertainty on mesh M2 is thus $e(X_R) = 100 \times |X_{R2} - X_R^*| / X_R^* = 0.10\%$. Estimates for the uncertainty of C give values below 0.1% while the uncertainties of Ψ_R may reach higher values (above 1%, rising to about 10% at low ER).

4. Results and discussion

Results are presented here for the recirculation length, recirculation intensity (Ψ_R , the normalized stream function), velocity and stress profiles at various locations and the Couette correction. The recirculation intensity is the total flow rate inside the corner eddies in excess of the inlet channel flow rate and normalized by the inlet flow rate. It is calculated from integration of the stream function using its definition: $u = \partial\psi/\partial y \Rightarrow \psi_{j+1} = \psi_j + u_j \Delta y_j$; the maximum value of ψ in the flow domain is ψ_{\max} , the inlet value is ψ_{inl} (equal to the imposed flow rate per unit depth), and the definition of recirculation intensity is thus $\Psi_R = (\psi_{\max} - \psi_{\text{inl}}) / \psi_{\text{inl}} = \Psi_{\max} - 1$. The Couette correction represents the pressure drop across the expansion after subtracting the fully developed pressure difference (i.e., the extra pressure drop) assuming the flow is fully developed in the whole of each channel and normalized as

$$C \equiv \frac{\Delta p - \Delta p_{\text{fd}}}{2\tau_w}, \quad (4)$$

Table 2
Extrapolated data for x_R/D , Ψ_R and C as a function of ER and De .

De	x_R/D	Percent error	$\Psi_R \times 10^3$	Percent error	C	Percent error
(a) ER = 1.25						
0	0.1443	0.002	0.1415	0.21	0.07612	0.055
0.1	0.1429	0.07	0.1348	0.91	0.1186	0.045
0.2	0.1414	0.08	0.1253	1.0	0.1588	0.045
0.3	0.1412	0.08	0.1191	0.85	0.1981	0.055
0.4	0.1422	0.08	0.1170	1.4	0.2369	0.051
0.6	0.1463	0.06	0.1217	6.4	0.3137	0.0091
(b) ER = 1.5						
0	0.2199	0.02	0.3395	0.31	0.1573	0.030
0.1	0.2175	0.07	0.3216	0.62	0.2139	0.032
0.2	0.2138	0.10	0.2975	1.3	0.2660	0.032
0.3	0.2113	0.09	0.2776	1.0	0.3157	0.031
0.4	0.2108	0.10	0.2692	1.7	0.3639	0.025
0.5	0.2118	0.09	0.2666	1.9	0.4114	0.013
0.6	0.2141	0.11	0.2731	4.1	0.4583	0.0093
0.8	0.2211	0.30	0.3034	12	0.5508	0.051
1.0	0.2298	0.58	0.3098	16	0.6429	0.059
(c) ER = 2						
0	0.2957	0.01	0.6487	0.37	0.2588	0.015
0.1	0.2928	0.04	0.6224	1.2	0.3240	0.018
0.2	0.2865	0.05	0.5653	1.4	0.3824	0.018
0.4	0.2746	0.01	0.4665	0.71	0.4881	0.013
0.6	0.2695	0.05	0.4309	1.6	0.5861	0.016
0.8	0.2697	0.13	0.4395	4.8	0.6792	0.066
1.0	0.2746	0.16	0.4858	12	0.7705	0.081
(d) ER = 3 ^a						
0	0.3531	0.08	0.9967	0.17	0.3412	0.18
0.2	0.3449	0.44	0.8758		0.4682	
0.4	0.3286	0.43	0.7022		0.5761	
0.6	0.3142	0.61	0.5742		0.6746	
0.8	0.3002	0.09	0.4874	0.41	0.7668	0.27
1.0	0.2937	0.28	0.4514		0.8555	
(e) ER = 4						
0	0.3750	0.04	1.1756	0.059	0.3738	0.040
0.2	0.3681	0.04	1.0791	0.72	0.5033	0.036
0.4	0.3534	0.04	0.8813	0.062	0.6107	0.021
0.6	0.3364	0.02	0.7035	0.43	0.7073	0.00094
0.8	0.3208	0.05	0.5706	0.66	0.7968	0.060
1.0	0.3073	0.10	0.4754	1.3	0.8809	0.13
(f) ER = 8						
0	0.4006	0.004	1.4498	0.22	0.4052	0.034
0.2	0.3972	0.001	1.3886	0.30	0.5350	0.030
0.4	0.3896	0.03	1.2616	0.51	0.6425	0.017
0.6	0.3804	0.02	1.1117	0.035	0.7389	0.0059
0.8	0.3703	0.05	0.9702	0.45	0.8280	0.062
1.0	0.3601	0.08	0.8456	0.82	0.9114	0.12
(g) ER = 16						
0	0.40976	0.02	1.5850	0.27	0.4133	0.035
0.2	0.40813	0.02	1.5532	0.32	0.5431	0.031
0.4	0.40463	0.0008	1.4784	0.11	0.6505	0.018
0.6	0.40012	0.002	1.3946	0.13	0.7469	0.0035
0.8	0.39523	0.02	1.3059	0.17	0.8359	0.061
1.0	0.39045	0.03	1.2274	0.088	0.9195	0.12
(h) ER = 32						
0	0.41369	0.02	1.6506	0.13	0.4153	0.036
0.2	0.41288	0.02	1.6320	0.051	0.5451	0.031
0.4	0.41146	0.04	1.5956	0.068	0.6526	0.018
0.6	0.40891	0.02	1.5508	0.10	0.7489	0.0049
0.8	0.40651	0.01	1.5021	0.080	0.8381	0.057
1.0	0.40456	0.03	1.4529	0.12	0.9216	0.12

x_R/D and C – extrapolation by Richardson's technique for second order of accuracy; Ψ_R – extrapolation by Richardson's technique for first order of accuracy.

^a Includes data from [16].

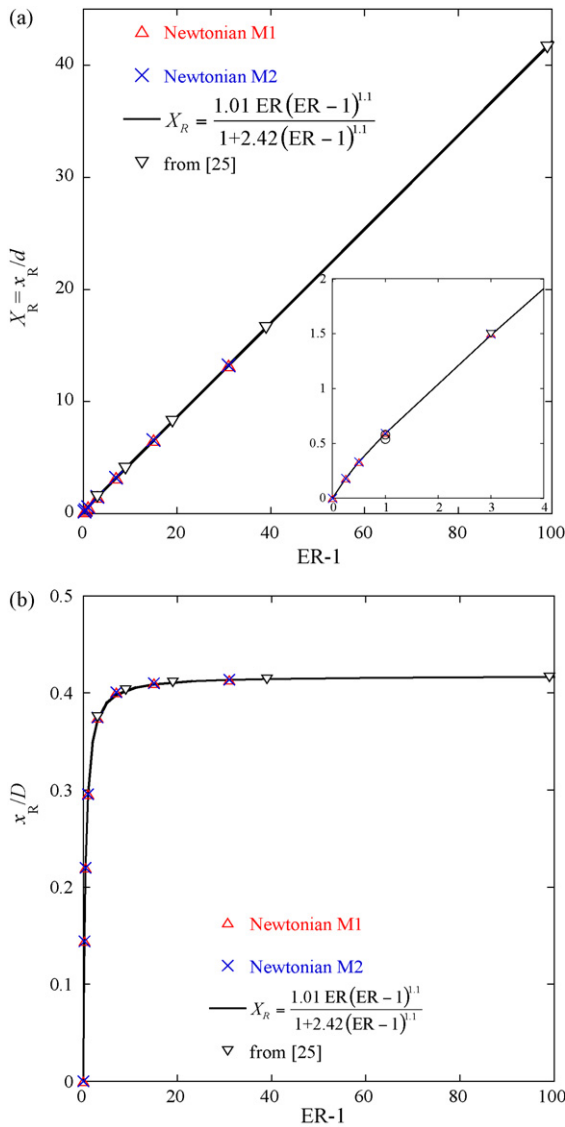


Fig. 2. Variation of the recirculation length with expansion ratio for Newtonian fluids: (a) x_R/d for $0 \leq ER - 1 \leq 31$ (inset for $0 \leq ER - 1 \leq 3$; (○) from [23,24]); (b) x_R/D .

where τ_w is the wall shear stress of the fluid in the fully developed inlet channel flow ($\tau_w \equiv 3\eta U_B/d$). In addition, streamline plots and contour plots of the stress fields are shown to help visualize the flow dynamics. At the end we discuss the issue of convergence and its relation to the maximum Deborah number where steady flow is predicted. Only creeping flow (i.e., $Re \rightarrow 0$) is considered in this work.

4.1. Newtonian fluid

The variation of the recirculation length (x_R) with expansion ratio (ER) for Newtonian fluids is plotted in Fig. 2 together with the correlation:

$$\frac{x_R}{D} = \frac{1.01(ER - 1)^{1.1}}{1 + 2.42(ER - 1)^{1.1}}. \quad (5)$$

This correlation fits the predictions nicely, with an average error of 0.4% and a maximum error of 0.9% for $ER = 4$. When normalizing with the upstream half-width, this variation is linear for $ER \geq 4$, as shown by the asymptotic behavior of the fitting in Fig. 2(a) for

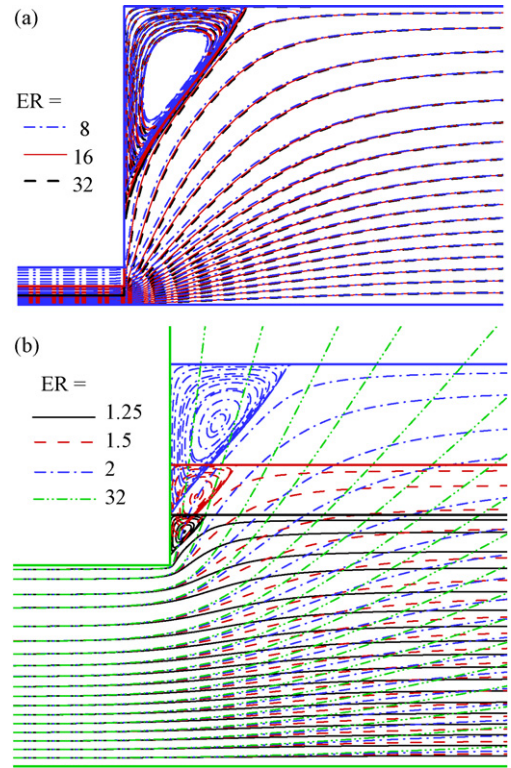


Fig. 3. Streamline plots for Newtonian fluids: (a) normalization with downstream quantities ($ER = 8, 16$ and 32); (b) normalization with upstream quantities ($ER = 1.25, 1.5, 2$ and 32). (For interpretation of the references to color in this figure legend, the reader is referred to the web version of the article.)

large values of ER ($x_R/d \sim 0.417ER$), and it is non linear for very small recirculation lengths as shown in the inset. Data from the literature for Newtonian creeping flow is scarce and we could only find information in Hung and Macagno [23,24] for $ER = 2$, who provided the values $X_R = x_R/d = 0.58$ and 0.54 , respectively, plotted in the inset. However, because the Newtonian creeping flows are linear and reversible contraction flow data must be identical, representative data from the literature [25] is also included for comparison. The linear variation of $X_R = x_R/d$ at large ER expresses a dependence of x_R almost exclusively on the size of the outlet channel, whereas the behavior at low ER must convey the disappearance of the recirculation as ER decreases to zero (in a planar channel). This behavior is better seen in the plot of Fig. 2(b), where x_R is now plotted normalized with D . It is clear here that for expansion ratios in excess of 8 the flow dynamics essentially depends on the step size (or on the outlet channel width). The $ER = 4$ case is intermediate between the high and low ER. A linear extrapolation of the large ER behavior to $ER = 1$ results in a finite size of the recirculation, but as ER decreases towards one the separation should vanish because the fluid has always some capacity to negotiate the corner against a vanishing small adverse pressure gradient, as is well shown in the figure and by the recommended fitting.

The difference between low and high expansion ratio behavior is also apparent in the streamline plots of Fig. 3. In Fig. 3(a) we compare streamline plots for different large expansion ratios where we have scaled the dimensions of the geometries in order to match the outlet channel widths. It is clear that the streamlines at large ER essentially collapse in the outlet channel, thus justifying the plateau observed in Fig. 2(b). In Fig. 3(b) the inlet channels have the same width and we see a fast reduction in the recirculation streamlines as ER decreases. In creeping flow of viscoelastic fluids through sudden contractions, Alves et al. [25] and Oliveira et al. [26] also reported the existence of different controlling variables in the dynamics of

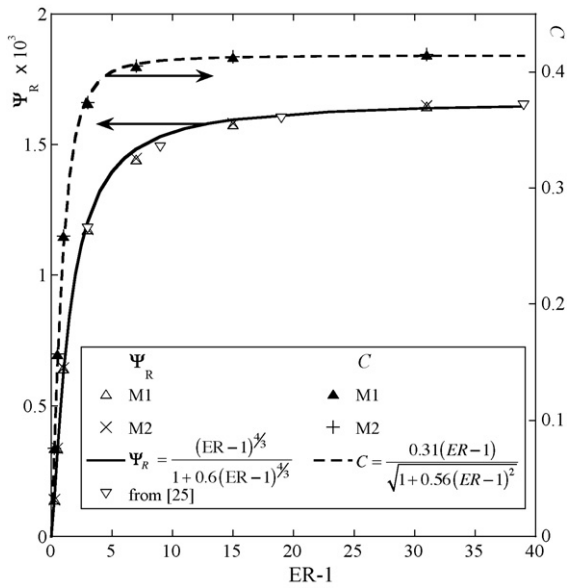


Fig. 4. Variation of recirculation intensity and Couette correction with expansion ratio for Newtonian fluids.

the recirculation at low and high contraction ratios, respectively for planar and axisymmetric geometries.

The corresponding variations of the recirculation intensity and of the Couette correction are plotted in Fig. 4. The variation of Ψ_R with $ER - 1$ shows a plateau at large expansion ratios in agreement with the plot of x_R/D in Fig. 2(b), thus confirming that the vortex is essentially controlled by the step size except at small expansion ratios, where the inlet channel also has some influence. When $ER - 1$ decreases toward zero Ψ_R also vanishes, and the following correlation is valid for the whole range of ER with an average discrepancy of 2% and the correct asymptotic behaviors at low and high $ER - 1$:

$$\Psi_R = \frac{(ER - 1)^{4/3}}{1 + 0.6(ER - 1)^{4/3}}. \quad (6)$$

Regarding the pressure losses for Newtonian creeping flow measured by the Couette correction (C) the trend is similar to that for the vortex intensity as illustrated by the dashed lines in Fig. 4. The Couette correction levels off at about 0.416 at large expansion ratios (cf. Fig. 4) and should obviously tend to zero as the expansion tends to a straight channel, because it represents the extra loss due exclusively to the expansion. The following correlation is valid for the whole range of expansion ratios and the average difference with the Couette correction data is 1.9%:

$$C = \frac{0.31(ER - 1)}{\sqrt{1 + 0.56(ER - 1)^2}}. \quad (7)$$

Eqs. (5)–(7) are recommended for the calculation of eddy size, eddy intensity and Couette correction in Newtonian creeping flow through planar expansions of varying expansion ratio. At high expansion ratios ($ER \gg 4$), physical reasoning suggests a simple dependence of those parameters with $(ER - 1)$ and in this case the following correlations are an approximation of the previous formulae which fit well this upper ER -range: $x_R/d = 0.417(ER - 1) + 0.263$; $\Psi_R = 1.71 - 1.97/(ER - 1)$; $C = 0.416 - 0.059/(ER - 1)$.

4.2. Viscoelastic flow

The flow characteristics of viscoelastic fluids are more complex as they combine the high versus low expansion ratio properties with specific elastic effects which also differ at high and low ER . To

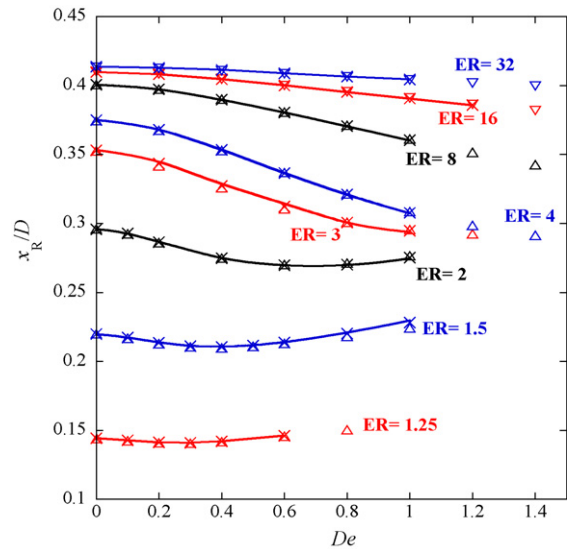


Fig. 5. Variation of the recirculation length x_R/D with expansion ratio and Deborah number for UCM fluids: (\triangle) mesh M1; (\times) mesh M2; (solid line) extrapolated data.

best visualize all these effects x_R/D is plotted in Fig. 5 as a function of De for the whole range of ER studied, with this parameter spanning both the low and high ER range.

There are several distinguishing features in Fig. 5. At large expansion ratios ($ER \geq 4$) x_R/D is a decreasing function of De , whereas at low values of ER ($ER < 3$) there is a non-monotonic variation with x_R/D initially decreasing with De followed by an increase. The sensitivity of x_R/D to viscoelasticity also decreases with ER ; the variations with De at $ER = 32$ are smaller (of the order of 3% for $0 \leq De \leq 1$) than at lower ER (at $ER = 4$ the corresponding variation of x_R/D with De is of the order of 20%). For $ER < 4$ the variations of x_R/D are also significant, but because of the non-monotonic behavior small differences are quantified when, say, comparing values at $De = 0$ and 1. Sensitivity to mesh refinement is also illustrated in Fig. 5 with essentially imperceptible distinctions between the recirculation length predicted on the two meshes except at large De for the smaller expansion ratios where small differences are visible. Table 2 presents the extrapolated data to facilitate future comparisons. These data were calculated with Richardson’s extrapolation

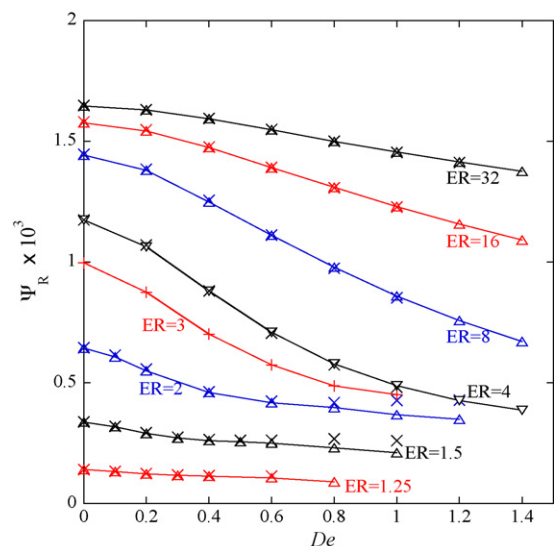


Fig. 6. Variation of the recirculation intensity with expansion ratio and Deborah number for UCM fluids: (\triangle and lines) mesh M1; (\times) mesh M2.

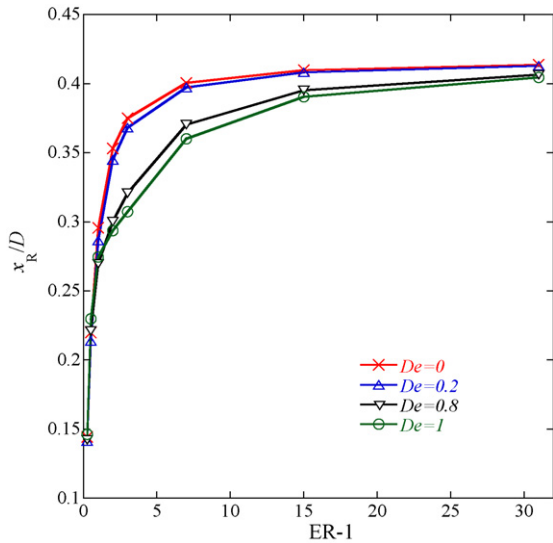


Fig. 7. Variation of the recirculation length x_R/D with expansion ratio for UCM fluids.

technique assuming second order accuracy based on an assessment done for contraction flow [25] and a few numerical experiments in the sudden expansion geometry.

The behavior of x_R/D is somewhat mimicked by that of the recirculation intensity plotted in Fig. 6. For the smaller expansions Ψ_R decreases initially at low values of De followed by an increase as De approaches its maximum value, whereas at large expansion ratios there is a continuous decrease of Ψ_R with De , which becomes less pronounced as ER increases. However, the non-monotonic variation of Ψ_R at low ER is less pronounced than that of x_R/D . Additionally, the accuracy in Ψ_R is lower than that of x_R , because it is an integral quantity obtained by a lower order sum of mass fluxes thus introducing some cumulative effects on the global error (extrapolation of Ψ_R is calculated as $\Psi_R = 2\Psi_{R1} - \Psi_{R2}$, i.e., assuming first-order accuracy, where Ψ_{R1} and Ψ_{R2} refer to meshes M1 and M2, respectively). This shows as somewhat larger differences between results pertaining to M1 and M2, which are also larger at low ER than at high ER . These differences are consistent with the fact that convergence of Ψ_R to the same level of accuracy as of x_R would require computations on finer meshes. The extrapolated Ψ_R data is listed also in Table 2. These data were obtained assuming first order accuracy.

For Newtonian fluids x_R/D tends asymptotically to a constant value as ER increases (cf. Fig. 2). This is also seen with viscoelastic fluids in Fig. 7, but progress to the asymptotic value is slower as the Deborah number increases. It is difficult to ascertain whether this asymptotic value is independent of the Deborah number since the investigation of this particular issue would require simulations at much higher expansion ratios for which the computations become prohibitively expensive. However, since the vortex size is then essentially controlled by flow conditions having rather low shear rates, thus reducing the influence of elasticity, the expectation is for x_R to be independent of De . In conclusion, there are clearly two different trends on the vortex behavior with elasticity and ER , and in the following the presentation and discussion of results will deal separately with the high and low expansion ratio cases.

4.2.1. High expansion ratios

The asymptotic nature of the vortex size characteristics at large ER is patent in Fig. 8 where x_R/D is plotted in semi-log coordinates against $De/(ER - 1)$. A limiting asymptotic curve, not plotted in Fig. 8, can be easily guessed as a negative-concavity curved line enveloping the predicted data at higher De . This suggests that the flow dynamics downstream of the expansion plane are controlled

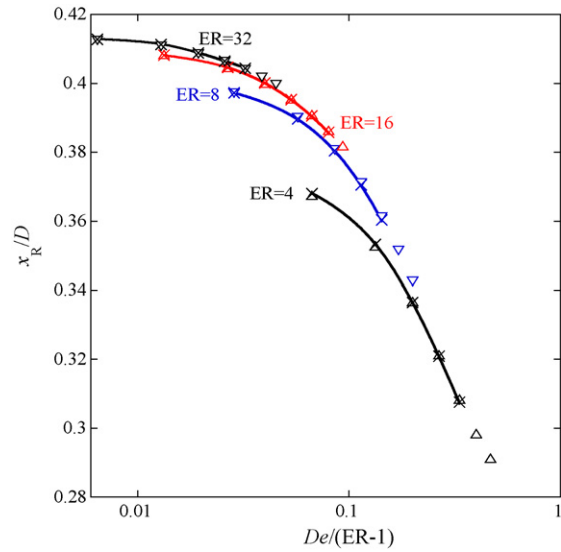


Fig. 8. Variation of the recirculation length x_R/D with $De/(ER - 1)$ at $4 \leq ER \leq 32$ for UCM fluids: (Δ and ∇) mesh M1; (\times) mesh M2; (solid line) extrapolated data.

by the step height in combination with an effect of Deborah number that tends to reduce the values of x_R/D . The streamline plots of Fig. 9 correspond to various high ER geometries and when normalized by the step size as in Fig. 9(b), there is a good level of correlation thus confirming the previous suggestion. The plots of Fig. 9(a) are for identical value of De , which brings an upstream effect and as a consequence the streamlines do not collapse. However, by plotting the streamlines at identical values of $De/(ER - 1)$, which is equivalent to an alternative Deborah number ($De' \equiv \lambda U_B/h$), we see the collapse of the flow streamlines. The exception is for $ER=4$ (green lines) which is on the borderline between high and low ER cases and

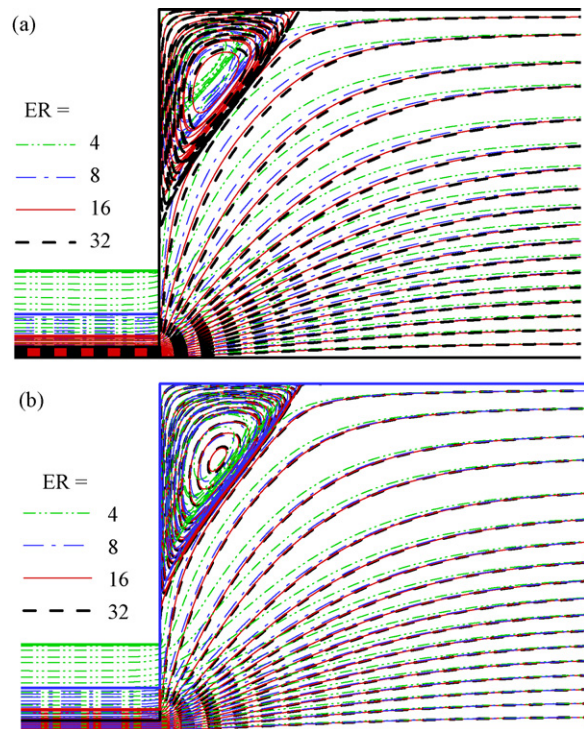


Fig. 9. Streamline plots for viscoelastic fluids at large expansion ratios ($4 \leq ER \leq 32$) normalized by the downstream channel size: (a) at $De=1$; (b) at $De/(ER - 1)=0.025$. (For interpretation of the references to color in this figure legend, the reader is referred to the web version of the article.)

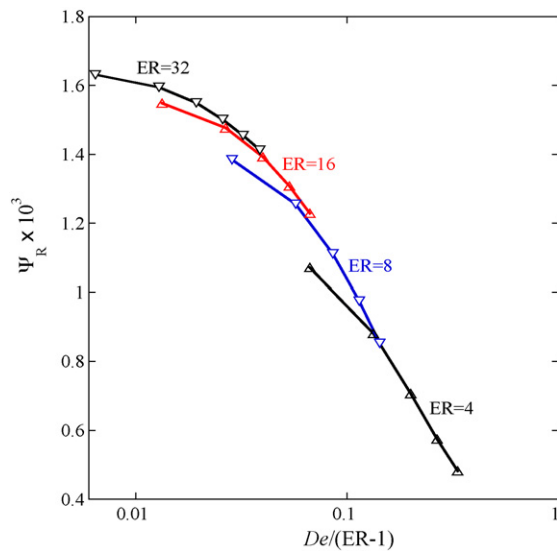


Fig. 10. Variation of recirculation intensity with expansion ratio and $De/(ER - 1)$ for $4 \leq ER \leq 32$.

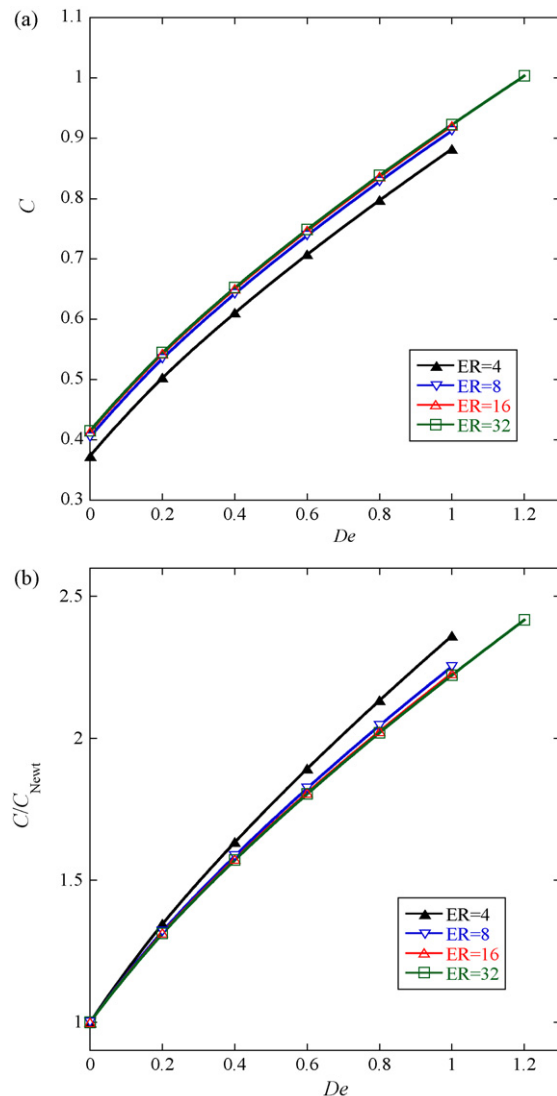


Fig. 11. Variation of the Couette correction with De and ER at large expansion ratio: (a) C versus De ; (b) C/C_{Newt} versus De .

does not show a large enough expansion ratio to behave asymptotically. Regarding the vortex intensity, the variations of Ψ_R with De and ER plotted in Fig. 10 show exactly the same asymptotic pattern as the variations of x_R/D in Fig. 8.

At large expansion ratios the Couette correction is also independent of ER as shown in Fig. 11(a), where data for $ER=8$ differ from data at $ER=32$ by less than 2.5% at $De=0$ and 1.2% at $De=1$. Since the extra pressure drop in C is normalized by inlet quantities (cf. Eq. (4)), the normalized pressure ($p/(\eta U_B/d)$) variation becomes independent of ER and is essentially that given for an exit flow at the same Deborah number, except for the very small contribution from the entry region. For $De=0$ this corresponds approximately to half the entry pressure drop for creeping flow through a rectangular orifice plate (a sudden contraction followed by a sudden expansion), a Sampson-like solution for the circular duct [27].

The other visible effect in Fig. 11(a) concerns viscoelasticity with C increasing with De with a linearly decreasing slope. This dependence of C on De also tends to be unique at large ER , here represented by $ER=32$, and given by

$$C = 0.416 + 0.645 De - 0.112 De^2 \quad (8)$$

with a correlation coefficient $r=0.9998$. This expression was obtained by fitting a parabola to Richardson's extrapolated data of C (denoted C^*) based on the calculated values of C on meshes M1 and M2, assuming second order accuracy, in accordance with previous work [22]. For example, for $De=1$ and $ER=4$ the Couette correction calculated on meshes M1 and M2 were: $C_1=0.88538$ and $C_2=0.88204$; Richardson extrapolation gives $C^*=(4C_2 - C_1)/3=0.88093$ and the uncertainty on mesh 2 is therefore $e(C_2)=100 \times |C_2 - C^*|/C^*=0.13\%$. Reducing the value of ER lowers the $C-De$ curve which is still parallel to the curves at larger ER . This shift of the $C-De$ curve implies that the relative variation of C with De is actually larger at low expansion ratios than at higher ER as shown in the plot of C/C_{Newt} of Fig. 11(b), where C_{Newt} is the corresponding Couette correction for Newtonian fluid flow presented in Section 4.1.

4.2.2. Low expansion ratios

At low expansion ratios there is no dominant influence as at high ER , and the flow characteristics are determined by the complex interactions between ER and the Deborah number. As a consequence, we observe the non-monotonic variation of the recirculation length with De already reported in Fig. 5, consisting of a decrease at low De followed by an increase at high De . These variations depend in a complex way on both ER and De and are better seen at intermediate values of ER , as exemplified by $ER=1.5$ and 2 . At low ER a simple scaling is not observed, even when the same data of Fig. 5 is plotted against $De/(ER - 1)$, and therefore the conclusion is that both the upstream and downstream duct sizes have an influence upon the vortex characteristics.

The relative amount of recirculating flow for $ER \leq 4$, as measured by Ψ_R , is plotted in Fig. 6 showing curves qualitatively similar to those of x_R/D , but the non-monotonicity is less obvious than for x_R , as already mentioned. It is necessary to look at the actual numerical values to confirm the tendency of Ψ_R to rise at high De (for $ER=1.5$ for example).

As at high expansion ratios the Couette correction increases with both the Deborah number and ER , as shown in Fig. 12(a). This corresponds to an enhanced pressure drop due to viscoelasticity, in opposition to the findings in the related contraction flows, where predictions with the UCM and similar viscoelastic models suggest a decrease of pressure losses while experiments nevertheless indicate a pressure loss enhancement. This plot includes also the curve pertaining to $ER=32$, which is essentially the high ER limit (cf. Fig. 11(a)). As for x_R/D a simple scaling does not exist for C . We see a reduction in C as ER decreases leading to C versus De curves shifting

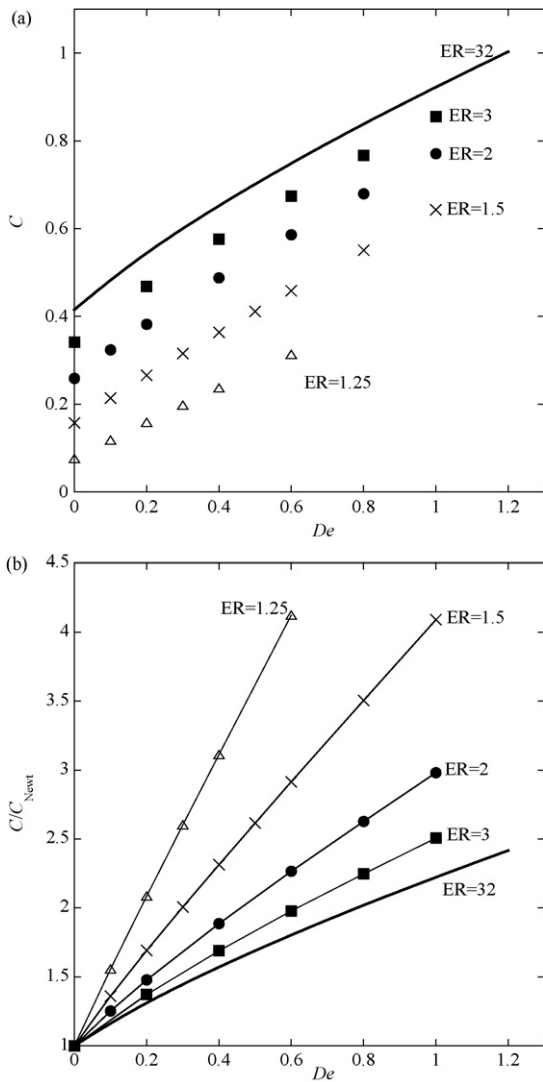


Fig. 12. Variation of the normalized pressure drop with De at low ER: (a) C ; (b) C/C_{Newt} .

downwards, but in relative terms there is a higher sensitivity to the Deborah number at lower expansion ratios as can be observed in the plots of C/C_{Newt} versus De of Fig. 12(b). The extrapolated data for C , determined assuming second order accuracy, are also listed in Table 2.

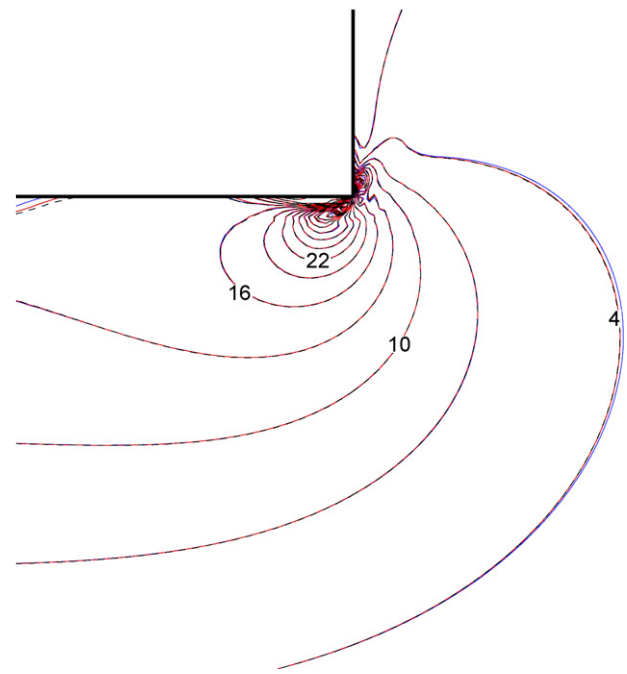


Fig. 14. Contours of $\tau_{xx}/(\eta U_B/d)$ in the vicinity of the re-entrant corner for $ER = 4$ (blue), 8 (red) and 16 (black) at $De = 1$. (For interpretation of the references to color in this figure legend, the reader is referred to the web version of the article.)

4.3. Flow at the maximum Deborah number

For all expansion ratios the simulations ceased to converge at Deborah numbers of the order of 1. This convergence problem was found to occur after a small vortex appears at the upstream duct wall near the re-entrant corner, as seen in the streamline plot of Fig. 13 for $ER = 4, 8$ and 16. To clarify that this is not a numerical artifact we performed a series of computations for the $ER = 4$ geometry using meshes finer than those in Table 1. We show at the inset of Fig. 13 that the lip vortex is well resolved on meshes M2 and M3 (cell sizes were halved when going from mesh M2 to mesh M3). We think these results provide sufficient evidence for the actual existence of the small lip vortex formed upstream of the expansion plane, whose presence was already pointed out in our previous paper [16], where it was linked with the formation of local convergence of the flow streamlines. In our view the viscoelastic fluid cannot turn the corner following the strong curvature imposed by the walls at 90° and is compelled to form a small eddy in order to reduce the local streamline curvature.

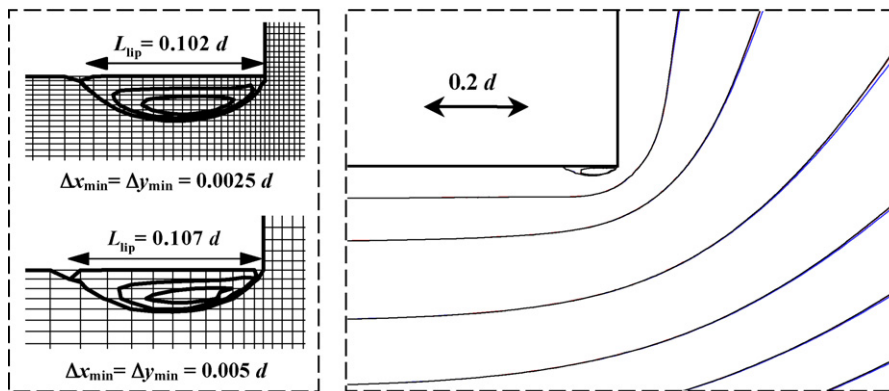


Fig. 13. Streamline plots in the vicinity of the reentrant corner for $ER = 4$ (blue), 8 (red) and 16 (black) at $De = 1$. The insets on the left correspond to a zoomed view of the lip vortex region, as predicted for $ER = 4$, on M2 and on a consistently refined mesh M3. (For interpretation of the references to color in this figure legend, the reader is referred to the web version of the article.)

At these flow conditions ($De \approx 1$) large extensional stresses develop in this small attached eddy as shown in the contour plots of Fig. 14, the streamlines show strong curvature (cf. Fig. 13) and large shear rates develop. Given these conditions, it might suggest the criterion for the onset of purely elastic instabilities of McKinley et al. [28,29] may be valid. In this criterion, at the onset of purely elastic instabilities it is postulated that

$$M \equiv \left[\frac{\lambda U}{R} \frac{\tau_{11}}{\eta \dot{\gamma}} \right]^{1/2} \geq M_{\text{crit}}, \quad (9)$$

where λ is the fluid relaxation time, U is the local fluid velocity, η is the zero shear rate viscosity of the fluid, $\dot{\gamma}$ is the local deformation rate, τ_{11} is the streamwise normal stress in the local flow direction and R is the local radius of curvature of the streamline. Calculations of τ_{11} and R were made following the procedure of Öztekin et al. [30]. The value of the critical parameter (M_{crit}) is specific to each flow problem and fluid type. Here we find that just before divergence the maximum local value of M^2 (hence an estimate of M_{crit}^2) takes a fairly constant value of around 4 for large expansion ratios, but it varies at low expansion ratios. The large ER behavior is consistent with the downstream scaling of the flow extensively discussed above and the collapse of the contours of M^2 (not shown here) is an obvious consequence of the collapsing contours of normal stress of Fig. 14. The maximum values of M^2 at $De = 1$ are 4.1 for $ER = 4$ and 4.2 for $ER \geq 8$.

In McKinley et al.'s [28,29] analysis there are steady stable two-dimensional base flows with curvature and large tensile stresses, which become disturbed at a certain critical Deborah number to end up as steady three-dimensional or unsteady flows. In the present work, the base stable flow is a complex combination of shear in the upstream channel and near walls, rotation near the two corners, and extension along the centreline, as can be inferred from a plot of a flow type parameter [31,32]. At $De \approx 1$ it gives rise to a second stable flow containing in addition a small lip vortex, and this flow diverges as De is further increased. In this second base flow, the lip vortex is still two-dimensional and it naturally gives rise locally to large stresses and large flow curvatures (flow curvature is the reciprocal of R). Clearly, more extensive studies require the use of different constitutive models to clarify this issue and to see whether flow divergence is preceded by the lip vortex, and what is the criterion for the onset of a lip vortex. Also, more investigation is required using an unsteady approach in the calculation of these flows around and above the critical Deborah number for unsteady flow.

5. Conclusions

The influence of expansion ratio upon viscoelastic flow through planar expansions has been studied numerically using the UCM constitutive model. For the creeping flow conditions considered, there is a scarcity of useful data in the literature, even for Newtonian fluids, which are a limiting case of the UCM model. Hence, for Newtonian fluid flows we provide data and useful correlations for the recirculation length and strength and the Couette correction. For the viscoelastic fluids in particular we have reported data characterizing the vortices formed downstream of the expansion plane and concluded that elasticity affects the flow differently depending on the expansion ratio. For high expansion ratios ($ER \geq 4$) the usual attenuation of vortex activity with elasticity is found, with recirculation sizes and local streamlines scaling with downstream channel width and a Deborah number defined as $De/(ER - 1)$ (where $De = \lambda U_B/d$). In contrast, for low expansion ratios ($ER \leq 3$) the recirculation size and intensity first decrease with De , before increasing again at high elasticity; this trend is more pronounced for the vortex size than for the intensity. Furthermore, in this low ER range there appears to be no definite length scale characterizing the recirculat-

ing flow; neither d nor D offer good collapse of the size and intensity data, or enable an adequate definition of an alternative Deborah number.

We also provide local pressure loss data, presented as a Couette correction factor C , which increases with Deborah number and also with expansion ratio, in absolute terms, but decreasing with ER when C is normalized with the corresponding Newtonian values. For all expansion ratios steady flow solutions were unattained at Deborah numbers above a critical value of the order of one, after a small lip vortex formed at the upstream duct wall near the reentrant corner, leading to the local development of large normal stresses. Attention was applied to matters of numerical accuracy and mesh refinement to guarantee that the predicted data here presented have good quality (maximum uncertainty of 1% in X_R and C).

Acknowledgements

The authors acknowledge funding by FCT through project PTDC/EME-MFE/70186/2006. M.A. Alves, F.T. Pinho and R.J. Poole wish to thank British Council and the Portuguese Council of Rectors for funding from the exchange projects B35/08, B10/07 and B11/07. P.J. Oliveira gratefully acknowledges a sabbatical leave conceded by Universidade da Beira Interior.

References

- [1] A.O. Restivo, J.H. Whitelaw, Turbulence characteristics of the flow downstream of a symmetric, plane sudden expansion, *ASME J. Fluids Eng.* 100 (1978) 308–310.
- [2] W.J. Devenport, E.P. Sutton, An experimental study of two flows through an axisymmetric sudden expansion, *Exp. Fluids* 14 (1993) 423–432.
- [3] W.H. Stevenson, H.D. Thompson, R.R. Craig, Laser velocimeter measurements in highly turbulent recirculating flows, *ASME J. Fluids Eng.* 106 (1984) 173–180.
- [4] R.J. Poole, M.P. Escudier, Turbulent flow of a viscoelastic shear-thinning liquid through a plane sudden expansion of modest aspect ratio, *J. Non-Newt. Fluid Mech.* 112 (2003) 1–26.
- [5] O.S. Castro, F.T. Pinho, Turbulent expansion flow of low molecular weight shear-thinning solutions, *Exp. Fluids* 20 (1995) 42–55.
- [6] A.S. Pereira, F.T. Pinho, Turbulent characteristics of shear-thinning fluids in recirculating flows, *Exp. Fluids* 28 (2000) 266–278.
- [7] R.J. Poole, M.P. Escudier, Turbulent flow of viscoelastic liquids through an axisymmetric sudden expansion, *J. Non-Newt. Fluid Mech.* 117 (2004) 25–46.
- [8] W. Cherdron, F. Durst, J.H. Whitelaw, Asymmetric flows and instabilities in symmetric ducts with sudden expansions, *J. Fluid Mech.* 84 (1978) 13–31.
- [9] D. Drikakis, Bifurcation phenomena in incompressible sudden expansion flows, *Phys. Fluids* 9 (1997) 76–87.
- [10] E. Schreck, M. Schäfer, Numerical study of bifurcation in three-dimensional sudden channel expansions, *Comput. Fluids* 29 (2000) 583–593.
- [11] P. Neofytou, D. Drikakis, Non-Newtonian flow instability in a channel with a sudden expansion, *J. Non-Newt. Fluid Mech.* 111 (2003) 127–150.
- [12] P.J. Oliveira, Asymmetric flows of viscoelastic fluids in symmetric planar expansion geometries, *J. Non-Newt. Fluid Mech.* 114 (2003) 33–63.
- [13] R.J. Poole, M.P. Escudier, P.J. Oliveira, Laminar flow of a viscoelastic shear-thinning liquid through a plane sudden expansion preceded by a gradual contraction, *Proc. R. Soc. Lond. Ser. A: Math. Phys. Sci.* 461 (2005) 3827–3845.
- [14] G.N. Rocha, R.J. Poole, P.J. Oliveira, Bifurcation phenomena in viscoelastic flows through a symmetric 1:4 expansion, *J. Non-Newt. Fluid Mech.* 141 (2007) 1–17.
- [15] F.T. Pinho, P.J. Oliveira, J.P. Miranda, Pressure losses in the laminar flow of shear-thinning power law fluids across a sudden axisymmetric expansion, *Int. J. Heat Fluid Flow* 24 (2003) 747–761.
- [16] R.J. Poole, M.A. Alves, P.J. Oliveira, F.T. Pinho, Plane sudden expansion flows of viscoelastic fluids, *J. Non-Newt. Fluid Mech.* 146 (2007) 79–91.
- [17] M.S. Darwish, J.R. Whiteman, M.J. Bevis, Numerical modeling of viscoelastic liquids using a finite-volume method, *J. Non-Newt. Fluid Mech.* 45 (1992) 311–337.
- [18] K.A. Missirlis, D. Assimacopoulos, E. Mitsoulis, A finite volume approach in the simulation of viscoelastic expansion flows, *J. Non-Newt. Fluid Mech.* 78 (1998) 91–118.
- [19] A. Afonso, F.T. Pinho, Numerical investigation of the velocity overshoots in the flow of viscoelastic fluids inside a smooth contraction, *J. Non-Newt. Fluid Mech.* 139 (2006) 1–20.
- [20] J.G. Oldroyd, On the formulation of rheological equations of state, *Proc. R. Soc. Ser. A* 200 (1950) 523–541.
- [21] P.J. Oliveira, F.T. Pinho, G.A. Pinto, Numerical simulation of non-linear elastic flows with a general collocated finite-volume method, *J. Non-Newt. Fluid Mech.* 79 (1998) 1–43.

- [22] M.A. Alves, P.J. Oliveira, F.T. Pinho, A convergent and universally bounded interpolation scheme for the treatment of advection, *Int. J. Numer. Methods Fluids* 41 (2003) 47–75.
- [23] T.-K. Hung, E.O. Macagno, Laminar eddies in a two-dimensional conduit expansion, *La Houille Blanche* 4 (1966) 391–401.
- [24] E.O. Macagno, T.-K. Hung, Study of a captive annular eddy, *J. Fluid Mech.* 28 (1967) 43–64.
- [25] M.A. Alves, P.J. Oliveira, F.T. Pinho, On the effect of contraction ratio in viscoelastic flow through abrupt contractions, *J. Non-Newt. Fluid Mech.* 122 (2004) 117–130.
- [26] M.S.N. Oliveira, F.T. Pinho, P.J. Oliveira, M.A. Alves, Effect of contraction ratio upon viscoelastic flow in contractions: the axisymmetric case, *J. Non-Newt. Fluid Mech.* 147 (2007) 92–108.
- [27] S. Sisavath, X.D. Jing, C.C. Pain, R.W. Zimmerman, Creeping flow through an axisymmetric sudden contraction or expansion, *Trans. ASME J. Fluids Eng.* 124 (2002) 273–278.
- [28] P. Pakdel, G.H. McKinley, Elastic instability and curved streamlines, *Phys. Rev. Lett.* 77 (1996) 2459–2462.
- [29] G.H. McKinley, P. Pakdel, A. Öztekin, Geometric and rheological scaling of purely elastic flow instabilities, *J. Non-Newt. Fluid Mech.* 67 (1996) 19–48.
- [30] A. Öztekin, B. Alakus, G.H. McKinley, Stability of planar stagnation flow of a highly viscoelastic fluid, *J. Non-Newt. Fluid Mech.* 72 (1997) 1–29.
- [31] G. Mompean, R.L. Thompson, P.R. Souza Mendes, A general transformation procedure for differential viscoelastic models, *J. Non-Newt. Fluid Mech.* 111 (2003) 151–174.
- [32] G. Astarita, Objective and generally applicable criteria for flow classification, *J. Non-Newt. Fluid Mech.* 6 (1979) 69–76.